Evaluation of green synthesized Fe_2O_3@MnO_2(core/shell) nanoparticles as antibacterial and adsorbent material for heavy metals

Rand A. Hayder, and *Zainab J.* Shanan*

Department of Physics, College of Science for Women, University of Baghdad, Baghdad, Iraq

Abstract. In this research, a core /shell from Fe2O3@MnO2-Nanoparticale was manufactured by Leek leaf extract in greenway biosynthesis. This method works as a reducing and covering agent. Fe2O3@MnO2 NPs have been confirmed as an effective antibacterial agent for both Gram-positive and Gram-negative bacteria. Synthesized nanoparticles were more efficient against gram-positive bacteria than gram-negative bacteria, with corresponding values of (31, and 24 mm) for klebsiella pneumoniae and Escherichia coli. Adsorption of metals (Pb, Cr, Ni, and Cd) by Fe2O3@MnO2 NPs trapped in calcium alginate was examined for use as a contaminant removal from water for the first time in Iraq. The results showed that nanoparticles trapped by alginate adsorbed more than alginate alone, and thus the Fe2O3@MnO2 nanoparticles (NPs) were able to remove lead, chromium, nickel, and cadmium from aqueous solutions with adsorption rate ranging between (84-99) %. Characteristics of synthesized nanoparticles were studied using (UV-visible) -spectroscopy, X-ray diffraction (XRD), and transmission electron microscopy (TEM).

1 Introduction

Pollution from industrial waste, which uses heavy metals and their applications, is one of the environmental problems Contemporary[1]. Plant-mediated nanoparticle synthesis has received a lot of interest due to its many benefits, including being non-toxic, safe, and cost-effective, mostly being environmentally benign [2]. Methods for removing metal ions from aqueous solutions mainly involve physical techniques chemical and biological. Eco-friendly synthesis techniques (green method) have been applied to create inexpensive, energy-efficient, and non-toxic metallic nanoparticles[3-5].To remove metal ions from aqueous solutions, traditional methods were used. Such as chemical precipitation, filtration, ion exchange, electrochemical treatment, and fumigation[6]. Metals can become hazardous and dangerous to living organisms when concentrations reach certain thresholds[7]. the high-molecular-weight biopolymer based on calcium alginate, known as an ion-exchange resin. This resin has been shown to have extraordinarily high capacities and kinetics for

* Corresponding author: zainabjs_phys@csw.uobaghdad.edu.iq

binding heavy metal ions, and it has also demonstrated that it is rather stable under a variety of chemical and physical circumstances (such as mixing strength and pH) [8, 9]. Oxidation processes are reduced by iron oxide nanoparticles. Because iron (II/III) ions are present in iron oxide nanoparticles, which are considered to be non-toxic and biocompatible materials, there has been a lot of interest in these materials [5, 10, 11]. As a result, the aforementioned environmental issues can be resolved in the quick and affordable synthesis of core-shell nanoparticles with more stable characteristics by immobilizing MnO_2 ions on Iron oxide nanoparticles and employing plant extracts as reducing agents. In the current research, *leek* extract has been used as the basis for a green synthesis that does not involve any additional chemicals, toxic substances, or additional reducing agents. Then evaluation of the synthesized nanoparticles Fe_2O_3@MnO_2 NPs as adsorbent material for some heavy metals which pollutant Tigris River in Baghdad/ Iraq and as an antibacterial, whereas waterborne bacteria have the potential to cause many diseases.

2. Experimental part

2.1 Chemicals and Materials

Leaves leeks were collected from Baghdad, Iraq, (local market). Both manganous sulphate monohydrate ($MnSO_4.H_2O$) and (ferrous sulphate heptahydrate) $FeSO_4.7H_2O$ were purchased from Merck. De-ionized water was used to prepare the aqueous solutions.

2.2 Preparation of *leek* extract

Leek leaf was cleaned with tap water first, then washed with distilled water to remove dirty and grimy material. 10 grams of *Leek* leaf weighing, in order to create the extract, the plants were cut up and heated to 35°C for 60 minutes in a flask containing 100 ml of deionized water. The extract was kept in a sterile container at 4 °C for later use.

2.3 Synthesis of Fe_2O_3 nanoparticles

To synthesize iron oxide nanoparticles, gradually add 10 mL of leek leaf extract dropwise to 1 g of $FeSO_4.7H_2O$ (0.14 M ferrous sulfate chloride heptahydrate). Shaking the sample on a shaker incubator continuously for an entire day at a temperature of 35°C caused the green color to turn brown. Centrifuge the sample for 10 minutes at 3000 rpm and then wash it. The solution is placed in a ceramic bowl and heated at a temperature of 40 degrees Celsius for (8-10) hours to form Fe_2O_3 nano-iron oxide powder. They are then crushed to produce iron oxide nanoparticles into a light brown powder. As shown in Figure (1).

Fig. 1. Fe_2O_3 -NP_s powder by green synthesis.

2.4. Synthesis of Fe_2O_3@MnO_2 core-shell nanoparticles

A solution of 0.1 M,1 gm (manganese sulphate monohydrate), ($MnSO_4.H_2O$), was mixed with 10 ml of aqueous extract of *leek* leaves and shaken quickly at 30°C on a hot motor (10 minutes) and in the next step, the above was added to (1gm) of Fe_2O_3 NPs prepared in step 2.3 at 30 °C. The resulting reaction mixture was stirred for 10 minutes and then in an incubator for 24 hours. The final step was centrifugation and washing the sample with ethanol and deionized water, then drying at 65 °C for (6 -8) hr. to get a fine powder from Fe_2O_3@MnO_2 NPs.

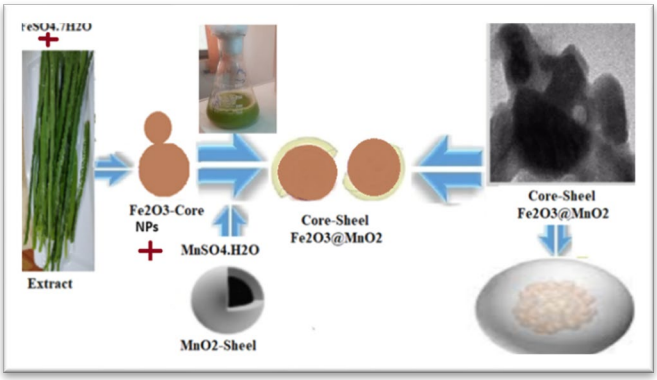

Fig. 2. Schematic green synthesis of Fe_2O_3@MnO_2 core-shell NPs.

2.5 Samples collection and their detection

Tigris River in the vicinity of the medical city hospital was selected as the site for the sample collection in the spring season. (1,300 -1350) yards from the point of the drain. Samples collected (10 to 30) centimeters under the surface of the water using sterile plastic bottles1.5-liter. The samples collected were kept around four degrees Celsius to preserve their properties while testing the ability of nanoparticles to inhibit bacteria. All of the colonies that formed on agar plates were identified after a 24-hour incubation period at 37°C by the application of standard bacteriological procedures with the use of a sterile swab, all isolates were streaked on chrome agar surface. It was found that pink, and blue colonies represent gram-negative (*E. coli and K. pneumoniae*) and white colonies of gram-positive represent Staph. aureus as depicted in figure (3).

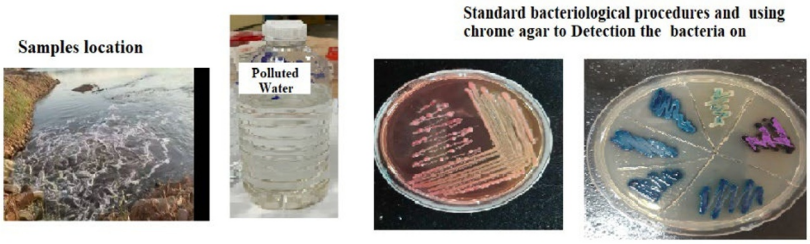

Fig. 3. Detection of bacteria on chrome agar from water pollution location.

3 Antibacterial activity of Fe_2O_3@MnO_2 NPs

The antibacterial activities of Fe_2O_3@MnO_2 nanoparticles were investigated via the well-diffusion method with both gram-positive (Escherichia coli) and gram-negative (*Escherichia coli, klebsiella pneumoniae*) bacteria [12, 13]. After mixing hot distilled water with muller agar, it was allowed to cool down to a temperature between 40° and 45° C after autoclaving. After that, MHA medium was regularly added to sterilized petri dishes, filling them to a depth of 5 mm[14]. It was decided to let the MHA medium cool to a normal temperature. (1.5 X 10^8 CFU/mL) was the benchmark for bacterial cultivation. A bacterial culture lawn was generated by spreading 50 µL of cultured broth and seeded (MHA) media with a 24-hour-old bacterial strain culture. Spread the bacteria onto the media using a glass spreader. Wells with a size of 6 mm were bored into the agar. Once every well on the plates was labeled, a micropipette was used to add 100 µg/ml of the Fe_2O_3@MnO_2 nanoparticle solution sample. Plates underwent a 24-hour incubation period at 37°C. After 24 hours, the plates were examined. It was found that all the concentrations were susceptible to all bacterial strains. In this case, we mostly display their results in (Table 1).

Table 1. Antibacterial activity for Fe_2O_3@ MnO_2 NPs.

Microorganisms	Zone of inhibition (mm)				
	(1000) µg/ml	(500) µg/ml	(250) µg/ml	(125) µg/ml	(62.5) µg/ml
Escherichia coli (−)	24	20	13	6	0
klebsiella pneumoniae (−)	31	23	19	13	6
staphylococcus aureus (+)	33.5	27	17	13	6

The Fe_2O_3 @MnO_2 NPs were effective as antibacterial, and from the zone inhibition area of bacteria, we notice that there are two regions for inhibition core with brown color for Fe_2O_3 and the shell with white color for MnO_2, which confirms the synthesis of core-shell (Fe_2O_3@MnO_2) NPs using the green method. With a zone of inhibition of (33 mm) for *staphylococcus aureus*, Fe_2O_3@MnO_2 nanoparticles were more efficient against gram-positive bacteria than gram-negative bacteria, with corresponding values of (31, 24 mm) for *klebsiella pneumoniae* and *Escherichia coli*. according to Figure (4)[12].

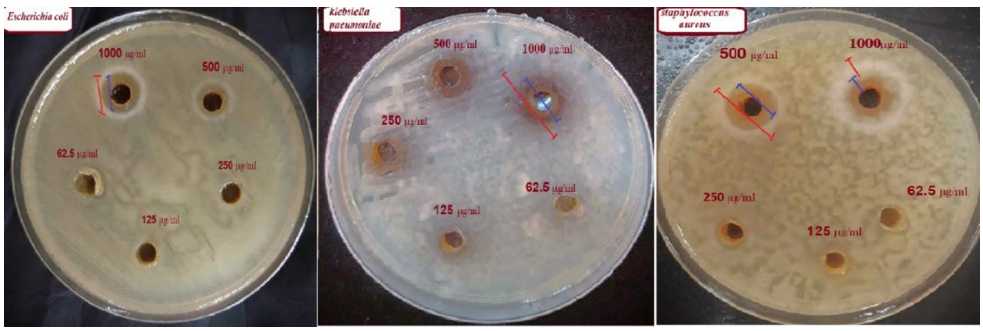

(a) (b) (c)

Fig. 4. Antibacterial activity of Fe_2O_3@MnO_2 NPs.

3.1 Results of antibacterial activity in the columns of calcium alginate beads and Fe_2O_3@MnO_2 NPs trapped in calcium alginate beads

Many types of bacteria, including gram-positive (Staphylococcus aureus), and gram-negative (klebsiella pneumoniae and Escherichia coli), were eliminated using nanoparticles [15]. A 200-microliter sample of the polluted water was taken and cultured in a plate before and after treatment from the two columns, and a test was conducted to remove bacteria from the water. It turned out that the number of bacteria before treatment was so large that it could not be counted, and after treatment, the bacteria were eliminated by up to 99%. This indicates the effectiveness of the synthesized nanoparticles in killing bacteria present in water. As shown in the figure 5 below.

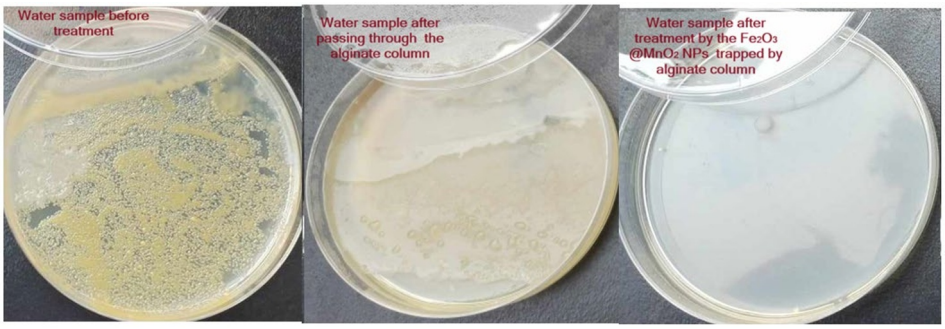

Fig. 5. Water sample before and after treatment.

4 Adsorption of Heavy metals

Adsorption of heavy metals from polluted water was studied using Calcium alginate (Entrapment material) and Fe2O3 @MnO2 (core-shell) NPs trapped by Calcium alginate.

4.1 Preparing of calcium alginate material (Entrapment material)

Three grams of sodium alginate were dissolved in 100 milliliters of distilled water to make the mixture which was then autoclaved at 121˚C for (15 min) and cooled down to 35 oC for experimental use. After obtaining the mixture, it was dropped carefully through a sterile syringe into a (0.2M) CaCl2 solution which was made by dissolving about 2.2 grams of CaCl2 in 100 milliliters of D.W to create tiny beads with a diameter from (1-4) mm. As shown in the figure (6).

Fig. 6. Entrapment material of calcium alginate beads.

4.2 Preparing of Fe_2O_3 @MnO_2 (core-shell) NPs trapped by calcium alginate

At a concentration of 500 µg/ml Fe_2O_3@MnO_2 nanoparticles were mixed with sterile sodium alginate solution. The mixture was stirred gently for ten minutes then extruded dropwise through a sterile syringe (10 ml) into a 0.2 M $CaCl_2$ solution to form small beads (1 to 4 mm in diameter). Calcium alginate beads were cleaned using D.W. It was observed that the granules turned brown as a result of the entrapment of nanoparticles with calcium alginate, as shown in Figure (7)**.**

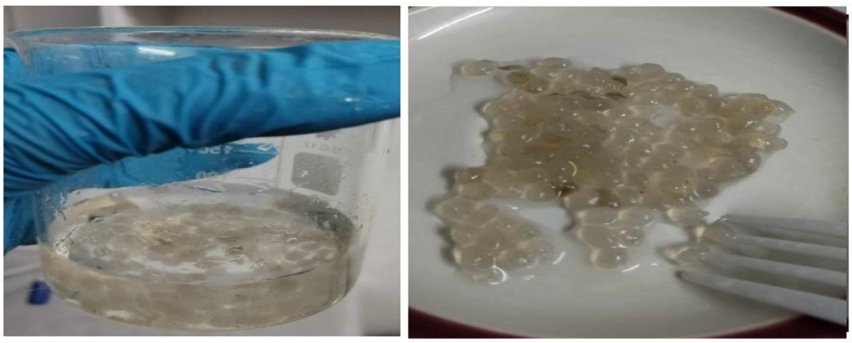

Fig. 7. Fe_2O_3@MnO_2 (core-shell) NPs Entrapped by calcium alginate beads.

4.3 Results of heavy metal adsorption columns by calcium alginate beads and Fe2O3@MnO2 NPs trapped in calcium alginate beads

Most of the metals were below the maximum contaminant level (MCL) for metals that can be found in drinking water based on the US Environmental Protection Agency and the World Health Organization [16]. 10 ppm (standard solution) for each of (lead, chromium Nickel, cadmium) was prepared in the laboratory for use with raw concentrations to study the efficiency of the nanomaterial for adsorption of heavy metals. Based on the results obtained, it appears that both Ca-alginate beads and Fe_2O_3@MnO_2 NPs trapped in Ca-alginate beads are effective in adsorbing heavy metals in columns. The polluted water was passed through two glass columns (with a diameter of 2 cm) to perform the adsorption process and the value of PH was equal to 5.5 as shown in Figure (7), the first for calcium alginate beads and the second for Fe_2O_3@MnO_2 nanoparticles trapped by calcium alginate beads. Table (2) shows the concentration of heavy metal ions (raw standard) for the sample studied before and after treatment and heavy metal concentration was examined in the two columns using an atomic absorption spectrometer. It was found that the heavy metals of lead, chromium, nickel, and cadmium were removed in a good proportion. The removal efficiency R and adsorption capacity q are calculated(table 3) using equations (1) and (2) [17]:

$$R = (C0 - Ce) \times 100/C0 \quad (1)$$

$$q = (C0 - C) \times V/M \quad (2)$$

where C0 (mg/L) and C (mg/L) are the initial and final pollutant concentrations in the solution, respectively. V(L) is the volume of the solution, and M(g) is the mass of the magnetic nanoparticles. The heavy metals were absorbed into the calcium alginate column by adsorption on the surface of natural porous materials, where the interaction between the adsorbent surface and the adsorbed particles is affected by the nature of the adsorbent material in terms of shape, size, polarity, solubility, etc. The difference between the

adsorbent surface and the adsorbed particles leads to selective adsorption for one of the components without the other. The ion exchange methods in the alginate column with low absorption capacity limit its applicability. Consequently, it is imperative to enhance alginate's adsorption capacity and stability of ion exchange, and their application in water treatment appears promising when combined with other potent adsorbents [13, 18, 19]. heavy metals in the column of Ca-alginate have been removed at a rate ranging from (13 to 8) %. the column of alginate with green nanoparticles demonstrated a higher removal rate of heavy metals compared to the alginate column alone. The results showed a high removal of heavy metals (lead, chromium) ranging between (99.8-98.8) % and (98.6-85) % for nickel and cadmium for the column of trapped nanoparticles. Research has demonstrated the effectiveness of utilizing nanoparticles in the treatment of wastewater. In some studies, iron oxide nanoparticles were found to be effective in removing different contaminants, such as cadmium and chromium, which were removed at a (100 to 99) % rate [14, 18].

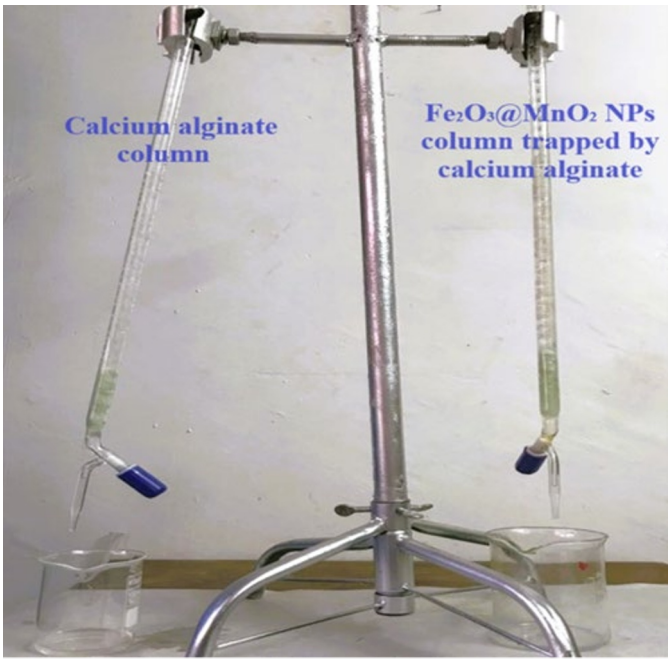

Fig. 8. Columns of calcium alginate beads and Fe2O3@MnO2 NPs trapped by calcium alginate beads.

Table 2. Heavy metals concentration of pollution water before and after treatment by alginate and Fe2O3@MnO2 NPs trapped by calcium alginate.

Concentration of Heavy metal ions in the raw Wastewater mg/l	Standard Concentration Prepare at the laboratory mg/l	Concentration After treatment by Ca-alginate mg/l	Concentration after treatment by Fe_2O_3@MnO_2 Trapped by ca-alginate mg/l
Pb = 0.08	10	**8.874**	0.0204
Cr = 0.017	10	**8.9712**	0.1209
Ni = 0.05	10	**8.9445**	0.1407
Cd = 0.016	10	**9.2147**	1.57

Table 3. Adsorption Capacity (q) and Removal efficiency (R) after and before treatment by Ca-alginate and Fe2O3@MnO2 NPs trapped by Ca-alginate.

Heavy metal elements in the Raw Wastewater and them Concentration mg/l	Standard Heavy Metals Concentration Prepare at the laboratory. mg/l	Adsorption Capacity (q) After Treatment by Ca-alginate (mg/g)	Adsorption Capacity (q) After Treatment by Fe_2O_3@MnO_2 + Ca-alginate (mg/g)	Removal Efficiency (R) After Treatment by Ca-alginate %	Removal Efficiency (R) After Treatment by Fe_2O_3@MnO_2 Ca-alginate %.
Pb = 0.08	10	**1.105**	**7.14**	**11.96%**	99.8%
Cr = 0.017	10	**0.924**	**8.53**	**11%**	98.8%
Ni = 0.05	10	**0.921**	**8.49**	**11%**	98.6%
Cd= 0.016	10	**0.66**	**6.03**	**8%**	84.3%

5 Characterization of Fe_2O_3@MnO_2 NPs

5.1 UV–vis spectrum characterization

UV-vis spectra were used to observe the synthesis of Fe2O3@MnO2 NPs core-shell. Figure 5 shows more than one absorption band, the optical absorption spectra of Fe2O3 NPs and Fe2O3@MnO2 NPs core-shell structure. The Fe2O3 NPs showed a distinctive SPR band at (298) nm, which is consistent with the literature reports [20]. there are two peaks of MnO2 that can be observed at (315 and 320) nm the peak of the core-shell has a good absorbent and is visible at (303) nm is attributed to (surface plasmon absorption), suggesting the development of a well-stabilized Fe2O3@MnO2 NPs core-shell structure. SPR of metallic nanoparticles is caused by a collective oscillation of conduction electrons over the metal NP surface. It has been observed that the addition of Mn salt and the formation of MnO2 reduces the intensity of Fe2O3 crystal absorption. This effect can be explained by a decrease in Fe2O3 nanoparticle absorption when a layer of MnO2 nanoparticles is present. That might result from changes to the particle sizes, surface microstructures, and morphologies [21].

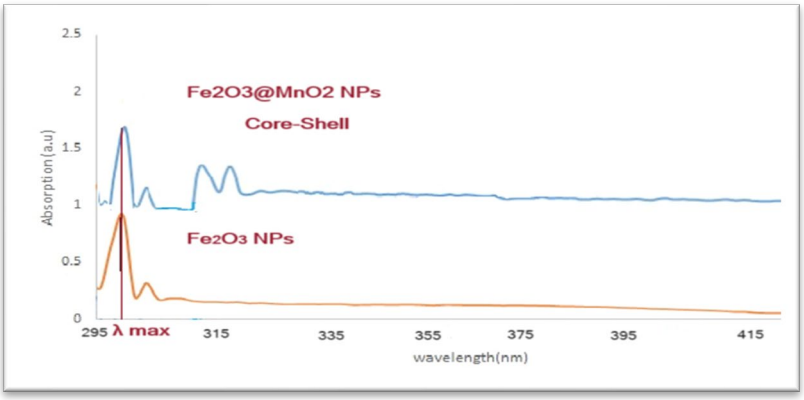

Fig. 9. UV-specter image of Fe2O3@MnO2-NPs and Fe2O3 NPs.

5.2 XRD characterization

X-ray diffraction spectroscopy (XRD) was conducted at a wavelength of (0.154 nm), and the crystalline of the green-produced Fe_2O_3@MnO_2 NPs were identified. The XRD spectra were captured in the range (10–80) °[22]. Fe_2O_3@MnO_2 NP samples were examined via X-ray diffraction (XRD), Figure (10) shows the XRD patterns of (Fe_2O_3@Mno_2) NPs which contain peaks of both crystalline Fe_2O_3 and MnO_2 NPs. Fe_2O_3 displayed peaks at 2θ values of 18.98° (100), 22.2° (012), 35.2° (110), 50.1° (024), and 61.3° (214) respectively[23]. The peaks at 2θ = 15.2°, 18.26°, 25.61°,32.71, and 72° can be indexed to the reflections of the (110), (200), (012), (104) and (222) crystalline planes of MnO_2 respectively[24]. Table (4) shows the crystal size values of Fe_2O_3@MnO_2 NPs with the highest intensity obtained by The Debye-Scherrer equation [23, 25, 26],

$$\text{Crystal size}(D) = k\lambda / \beta \cos\theta \quad (1)$$

Where (k): is the shape factor (0.94), (λ): is the incident radiation's x-ray wavelength (0.154252) nm, (β): (FWHM) is the full-width half maximum, and (θ): is the Bragg's angle, which takes into account the (X-ray) wavelength (0.154 nm), width of a peak with a maximum intensity in half height, the crystal's thickness (d), the diffraction angle, and the Debye-Scherrer constant (0.9). The mean crystalline size of Fe_2O_3 NPs is 41.46 nm and the mean crystalline size of MnO_2 NPs is 40.77 nm.

Table (4). crystalline sizes (D) of Fe_2O_3@MnO_2 Nanoparticles produced by green method.

NPs	2θ (Deg.)	(FWHM) (Deg.)	Crystalline size D(nm)	hkl
Fe_2O_3	**22.26**	0.35690	22.74	(012)
	35.2	0.16250	51.41	(110)
	50.1	0.17500	50.23	(024)
MnO_2	**18.26**	0.23640	34.12	(200)
	25.61	0.15750	51.85	(310)
	32.71	0.22820	36.36	(104)

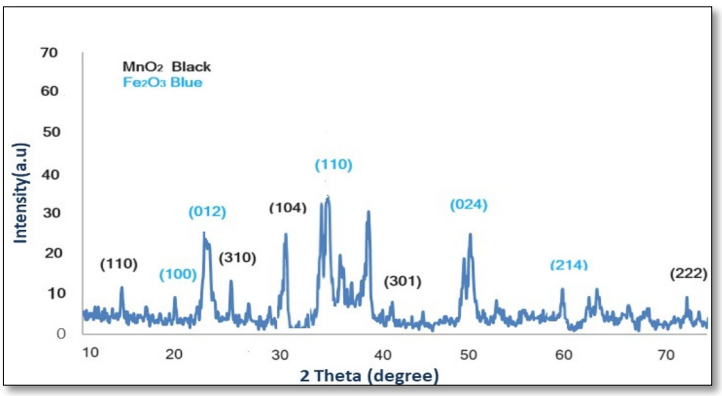

Fig. 10. XRD image of Fe2O3@MnO2 – NPs.

5.3 TEM characterization

TEM was employed to view the size and shape of the Fe2O3@MnO2 core-shell nanoparticles. The spherical shape of some particles and some agglomerated morphology is shown in Fig. (11) According to TEM data, some particles are less than 45 nm and others more than 100 nm. In this case, the gray shell is MnO2, and the black core is Fe2O3, the MnO2 shell thickness ranged from 5 to 12 nm. The benefits of a high-thickness shell include reduced iron core toxicity, high core/shell structural stability, and no oxidation of the iron core [27, 28].

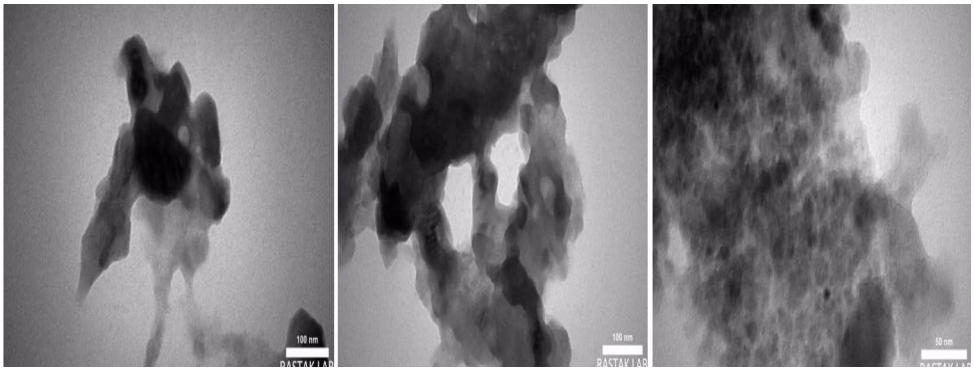

Fig. 11. TEM images of the prepared -Fe_2O_3@MnO_2 NPs.

6 Conclusion

In this study, Fe_2O_3@MnO_2 core/shell nanoparticles were synthesized using leek leaf extract. The nanoparticles were characterized by (UV-visible) spectroscopy, XRD, and TEM. The results demonstrated that these nanoparticles had the effect of removing heavy metals from wastewater, the results showed that nanoparticles trapped by alginate beads adsorbent heavy metals more than alginate beads alone, and thus the Fe_2O_3@MnO_2 nanoparticles were able to remove lead, cadmium, chromium, and nickel from aqueous solutions with an adsorption rate ranging between (84-99) % Moreover, Fe_2O_3@MnO_2 core/shell used in biological tests and showed how Fe_2O_3@MnO_2 nanoparticles affected both gram-positive and gram-negative water bacteria, and zone of inhibition of (33 mm) for staphylococcus aureus and Fe_2O_3@MnO_2 nanoparticles were more efficient against gram-positive bacteria than gram negative bacteria, with corresponding values of (31, 23 mm) for klebsiella pneumoniae and Escherichia coli.

References

1. S. Hembrom, et al., *A comprehensive evaluation of heavy metal contamination in foodstuff and associated human health risk: a global perspective,* Contemporary environmental issues and challenges in the era of climate change, 33-63 (2020).
2. A.S. Ertürk, G. Elmaci, and M.U. Gürbüz, Turkish Journal of Chemistry, **45**(6), 1968-1979 (2021).
3. Z.J. Shanan, S.M. Hadi, and S.K. Shanshool, Baghdad Science Journal, **15**(2), 0211-0211 (2018).
4. A. Khalid, H.H. Murbat, and Z.J. Shanan, Biochemical & Cellular Archives, **19**(2) (2019).

5. S.K. Shanshool, and Z.J. Shanan, Green Synthesis of Manganese Dioxide Nanoparticles and its Biological, Baghdad Science Journal (2023).
6. AAJ Aljanaby, ROMJ, **(7)1**, 1-6 (2018).
7. J.P. Chen, and H. Yu, Journal of Environmental Science & Health Part A, **35**(6), 817-835 (2000).
8. J.P. Chen, and J. Peng, Adv. Environ. Res, **3**(4), 439-449 (2000).
9. J.P. Chen, and L. Wang, Separation science and technology, **36**(16), 3617-3637 (2001).
10. A.A. Aljanaby, F.A. Gafil, Res Chem Intermed, **39(8)**, 3679-87 (2013).
11. S.K. Shanshool, and Z.J. Shanan, International Journal of Nanoscience, **22**(4), 2350030 (2023).
12. R. Hooda, and M. Sharma, Plant Arch, **20**(1), 1196-1200 (2020).
13. J. Raghuvanshi, R. Agrawal, and P. Ghosh, The Journal of Entrepreneurship, **26**(2), 220-238 (2017).
14. V. Jerin, et al., Materials Today: Proceedings, **9,** 27-31 (2019).
15. M. Diao, and M. Yao, Water research, **43**(20), 5243-5251 (2009).
16. M. Hashim, et al., Journal of environmental management, **92**(10), 2355-2388 2011..
17. C. Liosis, et al., Materials, **14**(24), 7500 (2021).
18. T. Hao, et al., Applied Surface Science, **292**, 174-180 (2014).
19. M. Víctor-Ortega, J. Ochando-Pulido, and A. Martínez-Férez, Separation and Purification Technology, **160,** 136-144 (2016).
20. P. Karpagavinayagam, and C. Vedhi, Vacuum, **160,** 286-292 (2019).
21. S. Azizi, et al., Applied Surface Science, 2016. **384**: p. 517-524.
22. R. Ali, et al., Iraqi Journal of Science, 266-276 (2020).
23. M. Balamurugan, S. Saravanan, and T. Soga, e-Journal of Surface Science and Nanotechnology, **12,** 363-367 (2014).
24. L. Christensen, et al., Advanced Materials Letters, **2**(6), 429-434 (2011).
25. Z.J. Shanan, N.K. Abdalameer, and H.M. Ali, International Journal of Nanoscience, **21**(03), 2250017 (2022).
26. S. Sabeha, and Z.J. Shanan, Ibn AL-Haitham Journal For Pure and Applied Sciences, **36**(3), 91-99 (2023).
27. H.Q. Alijani, et al., Biomass Conversion and Biorefinery, 1-15 (2022).
28. L. Shen, et al., Materials, **12**(5), 828 (2019).